Science & Technology Development Journal – Engineering and Technology 2024, 6(SI3):34-45

Open Access Full Text Article

Research article

Enhanced efficiency MnO_2-Promoted pt catalyst for VOCs oxidation

Khong Manh Hung*, Tran Van Hien, Ha Quoc Bang

ABSTRACT

One of the leading causes of air pollution, volatile organic compounds (VOCs) pose a severe danger to both the environment and human health. In heat or light, catalytic oxidation has been recognized as a promising and successful approach for treating VOCs. Due to their affordability and environmental friendliness, manganese-based oxides are one of the most competitive and acceptable choices for the catalytic destruction of VOCs. In this study, we disperse Pt on MnO_2 with trace Pt loadings of 0.5, 1, and 1.5 wt% to control the interaction of Pt-MnO_2 (MnO_2 = manganese oxide). In comparison to MnO_2, the Pt-MnO_2 catalyst exhibits higher VOCs oxidation performance due to its higher Brunauer-Emmett-Teller surface area, more active lattice oxygen, increased oxygen vacancy activating increased dioxygen molecules, more exposed Pt atoms, and noninternal diffusion of mass transfer. Among all the plantinum samples created with varying mass ratios, the Pt-MnO2 sample demonstrates the best characteristic characteristics as well as catalytic activity. The specific surface area of Pt-MnO2 is 108.74 m^2/g. The Pt-MnO_2 catalyst can totally convert Toluene into CO_2 and H_2O at a lower temperature of just 190 C while maintaining great stability for 600 minutes. Under conditions of high space velocity, the Pt-MnO_2 catalysts' performance in oxidizing VOCs is steady, indicating tremendous promise for real-world use. This research shows that a Pt-dispersed MnO_2 catalyst is superior to a MnO_2 catalyst for the oxidation of VOCs, offering universally significant advice for the interaction of metals with supports and the control of interfaces during oxidation processes. The results suggest that the synthesized Pt-MnO2 material has a comparatively strong capacity to oxidize VOCs at low temperatures and a high stability, and that it can be developed and scaled up to a wider application scale.

Key words: Manganese oxide, Platinum, Toluene, catalytic oxidation, VOCs

Institute of Chemistry and Materials, 17, Hoang Sam, Nghia Do, Cau Giay, HN 10000, Vietnam

Correspondence

Khong Manh Hung, Institute of Chemistry and Materials, 17, Hoang Sam, Nghia Do, Cau Giay, HN 10000, Vietnam

Email: Hungkhong123123@gmail.com

History

- Received: 2023-08-31
- Accepted: 2023-09-25
- Published Online: 2023-3-31

DOI :

https://doi.org/10.32508/stdjet.v6iSI3.1189

INTRODUCTION

The burning of fossil fuels, the volatilization of liquid fuels and solvents, and the emissions from chemical plants are the primary causes of VOCs emissions. In addition to being poisonous, carcinogenic, and mutagenic to humans, VOCs also threaten air quality by depleting the ozone layer and acting as precursors to photochemical smog. Thus, it is crucial to choose efficient VOCs pollution reduction strategies [1–3]. Diverse control strategies, including combustion, photocatalytic oxidation, adsorption methods, membrane separation, biotechnology, and catalytic oxidation, have been developed to limit the emissions of VOCs [4–7]. Catalytic oxidation has been regarded as one of the most promising techniques due to its high efficiency, energy conservation, and environmental friendliness [8,9]. The catalyst is often the most critical component in the low-temperature catalytic oxidation of VOCs. Noble metal-based catalysts are very effective in removing VOCs from the environment. However, their widespread use was hampered by their high cost, resource scarcity, and poor thermal stability. Contrarily, transition metal-based catalysts have gained popularity due to their inexpensive cost, strong thermal stability, and excellent oxygen storage capacity [10,11].

Transition metal oxide catalysts have demonstrated considerable potential in various applications owing to their advantageous characteristics such as cost-effectiveness, resistance to poisoning, and resistance to sintering [12,13]. Therefore, it is imperative to utilize transition metal oxide-based catalysts that exhibit elevated catalytic activity towards VOCs at reduced temperatures. There has been a growing interest in studying Co3O4, CeO2, and MnO2 in the past few years due to their well-defined and controlled nanostructures [14–16]. One notable example is MnO_2, which exhibits adjustable atomic valence states and crystalline phases. The catalyst based on MnO_2 is widely recognized for its high efficiency in converting ozone and its notable ability to adsorb VOCs and effectively activate oxygen at low temperatures [17–24]. According to the study conducted by Li et al., it was observed that α-MnO_2 exhibited a higher preference for the oxida-

Cite this article : Hung K M, Hien T V, Bang H Q. **Enhanced efficiency MnO_2-Promoted pt catalyst for VOCs oxidation**. *Sci. Tech. Dev. J. – Engineering and Technology* 2024; 6(SI3):34-45.

VNUHCM PRESS

tion of acetaldehyde and benzene to CO_2 compared to γ-MnO_2 and β-MnO_2. The phenomenon above can be ascribed to the favorable adsorption capacity and notable oxygen migration ability exhibited by α-MnO_2. In a study conducted by Liang et al., it was shown that MnO_2 with unique crystalline phases displayed varying levels of catalytic activity in the oxidation of CO. Specifically, δ-MnO_2, and α-MnO_2 exhibited superior catalytic performance compared to γ-MnO_2 and β-MnO_2 [24].

In recent years, numerous researchers have endeavored to augment the catalytic efficacy of catalysts based on MnO_2 by integrating additional metal species [25,26]. Several bimetallic catalysts, including Ag-Mn, Ni-Mn, and Ru-Mn, were synthesized specifically to degrade VOCs [27–30]. The introduction of an additional metal element not only influences the microstructural characteristics of MnO_2, such as specific surface area, crystallinity, and shape but also leads to synergistic effects that enhance the catalytic performance. The production of oxygen vacancies is facilitated by the interfacial active sites seen in both metal and metal oxide materials [31]. The proper cycling of dynamic oxygen species on the catalyst surface is critical in achieving deep oxidation of VOCs [32]. Moreover, it is widely acknowledged that Pt-based catalysts are the most preferred catalysts for the oxidation of VOCs at low temperatures [33,34]. In their study, Zhang et al. [35] employed Pt/MnO_2 as a catalyst for the oxidation of toluene. The results indicated that Pt/MnO_2 exhibited favorable catalytic activity under low-temperature conditions. The robust intermolecular interactions observed between manganese (Mn) and platinum (Pt) have been found to significantly augment the redox capability of catalysts composed of Pt/MnO_2. Thus, there is a strong demand for developing a Pt/MnO_2 catalyst that exhibits exceptional activity to enhance the oxidation of VOCs.

In this study, we provide a hydrothermal combinate approach combined with impregnation methods for synthesizing Pt/MnO_2. Our objective is to investigate the impact of the cation complex on the toluene oxidation process by altering the weight percentage of Pt at low temperatures. This study presents a proficient approach toward the component engineering of platinum and transition-metal oxides and their subsequent utilization in catalytic applications for the oxidation of toluene.

EXPERIMENT METHODS

Material

$MnSO_4.H_2O$, standard benzene solution, $KMnO_4$, PolyvinylPyrrolidone (PVP), Sodium Citrate ($Na_3C_6H_5O_7$), and L-Ascorbic acid were purchased from Xylong Ltd. Standard gas cylinders H_2, Ar, He, N_2, and O_2 are also used of domestic origin.

Preparation of catalysts

Synthesis of Manganese oxide MnO_2 TN

The experimental procedure involved the addition of 0.1 moles of potassium permanganate ($KMnO_4$) to a volume of 30 milliliters of distilled water. Subsequently, 0.15 moles of manganese sulfate ($MnSO_4$) solution was gradually added to the solution above. The resulting mixture was subjected to a heating process at ambient temperature for 4 hours, followed by transfer to an autoclave and further heating at 160 degrees Celsius for 3 hours. The liquid undergoes filtration, washing, and drying processes at a temperature of 80 ^{o}C on a nightly basis. The final product under consideration is manganese dioxide (MnO_2 TN) in its thermodynamically stable state.

Synthesis of Manganese oxide MnO_2 TN

The impregnation approach is utilized to carry Pt on top of MnO_2. To prepare solution A, 68 mg of PVP powder and 0.18 g of Sodium Citrate were dissolved in 100 ml of distilled water. To obtain solution B, 16mg of $H_2PtCl_6.6H_2O$ was dissolved in 10 milliliters of pure water. Gradually incorporate solutions B and A into the mixture and agitate for 5 minutes to obtain solution C. To obtain solution D, 10 ml of distilled water should dissolve 108 milligrams of ascorbic acid. The process of creating a Pt colloidal solution involves the gradual addition of D into solution C, followed by continuous stirring for a duration of 2 hours.

A solution containing 0.5 grams of MnO_2 dispersed in 50 milliliters of distilled water was exposed to ultrasonic vibration for 15 minutes. Subsequently, this solution was introduced into the Pt colloidal solution. The mixture should be stirred continuously and subjected to a temperature of 80 °C for a duration of 2 hours. The resultant product underwent filtration, followed by washing with distilled water and ethanol, and afterward underwent overnight drying at a temperature of 80 ^{o}C.

Furthermore, samples of $0.5Pt/MnO_2$ and $1.5Pt/MnO_2$ (with a mass percentage of Pt in the catalyst mixture of 0.5%w and 1.5%w, respectively) were synthesized using the same procedure described above. The only distinguishing factor between these entities is the variation of the precursor H_2PtCl_6's mass.

The synthesis process of Pt/MnO_2 is clearly illustrated in Figure 1.

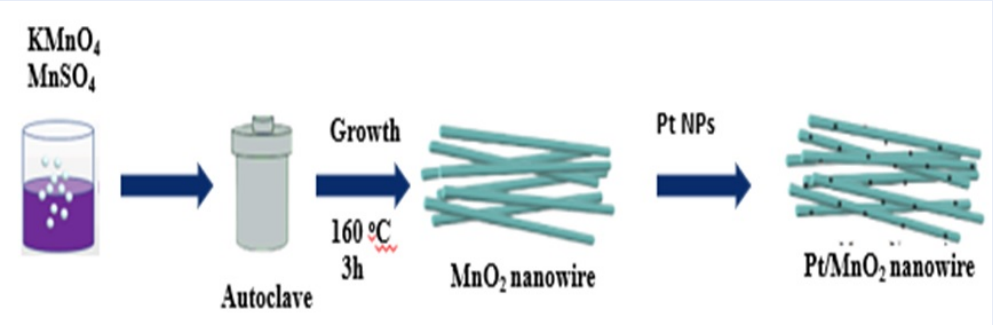

Figure 1: Flow chart of catalyst preparation of Pt/MnO_2.

Characterization of catalyst

The present work focused on analyzing catalyst morphology and microstructure by utilizing a scanning electron microscope (SEM) model Hitachi S-4800, manufactured in Japan. The chemical compositions and metal concentrations of catalysts were studied using a scanning electron microscope with an X-ray microprobe analyzer (EDS) spectrometer. The held samples were subjected to X-ray diffraction (XRD) analysis using D8 Advance Bruker equipment. The synthetic materials' Fourier Transform Infrared (FTIR) spectrum was examined in the wavenumber range of 400 to 4000 cm^{-1} using a reflection technique on a Bruker Tensor II instrument.

Measurement of catalytic activity

A micro-reactor system was employed for the remediation of benzene. The gaseous toluene was generated by adding nitrogen gas into liquid benzene via bubbling. Subsequently, it was subjected to a combination of N_2 and O_2. The flow rate of the entire mixture of reactants was established at 50 mL/min. Once the benzene concentration at the intake reached a steady state of 6,000 parts per million (ppm) and the gas hourly space velocity (GHSV) reached 11,000 h^{-1}. A quantity of 0.1 grams of each catalyst was placed at the center of a 60-centimeter-long reactor with a diameter of $\frac{1}{4}$ inch. The contents of CO_2 and benzene were determined by employing an online Focus-Thermo Scientific gas chromatograph equipped with a thermal conductivity detector (TCD) and a flame ionization detector (FID).

The benzene conversion ($X_{Toluene}$, %) was calculated using the following equation

$$X_T = \frac{C_T^1 - C_T^2}{C_T^1} \times 100 \quad (1)$$

Whereas:

X_T: Toluene conversion (%)

C_T^1: Toluene concentration of inlet flow at a temperature T (ppm);

C_T^2: Toluene concentration of inlet flow at a temperature T (ppm).

Meanwhile, the conversion of Toluene into CO_2 was determined as equation 2

$$\gamma_{CO_2} = \frac{C_{CO_2.T}^2}{6\left(C_T^1 - C_T^2\right)} \times 100 \quad (2)$$

Whereas:

$C_{CO2.T}^2$: CO_2 concentration of outlet flow at a temperature.

RESULTS AND DISCUSSION

Catalyst characterization

XRD spectroscopy was employed to examine the structural characteristics of the Pt/MnO_2 material. The XRD measurement findings for MnO_2 nanowire Pt/MnO_2 are shown in the following Figure 2.

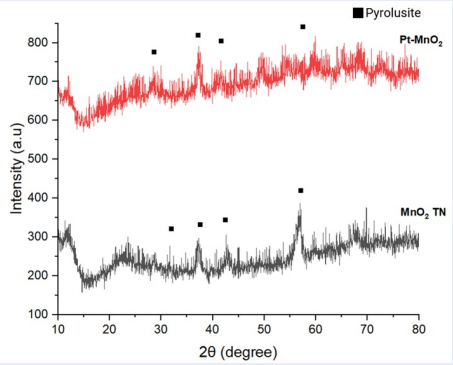

Figure 2: XRD pattern of MnO_2 and Pt/MnO_2.

Following the X-ray diffraction (XRD) characterization analysis, Pt peaks were not detected in the XRD

phase diagram. However, when Pt particles were introduced to the MnO_2 material, the intensity of the Manganese dioxide peaks decreased and became less distinct, as shown in the MnO_2 TN sample. Based on the XRD analysis, it is evident that the introduction of Pt metal onto MnO_2 does not induce any alterations in the phase structure of the material. This observation validates the complete preservation of the crystalline phase of MnO_2 while also indicating the uniform dispersion of Pt nanoparticles across the material's surface.

To further investigate the impact of the synthesis process on the creation of Pt/MnO_2 products, the synthesized sample underwent characterization using the Fourier Transform Infrared (FTIR) method throughout the wavelength range of 400 to 4000 cm^{-1}. The findings are presented in Figure 3.

Based on the Fourier Transform Infrared (FTIR) analysis of the two samples, it is evident that the introduction of Pt onto MnO_2 does not exert any discernible influence on the structural integrity of MnO_2. This is substantiated by the continued presence of the absorption band associated with Mn-O vibrations inside the MnO_x network, which remains observable within the wave number range of 400÷1100 cm-1. The observed shift in the absorption peak of the Pt/MnO_2 sample towards a lower wavelength (503.38 cm^{-1}) in comparison to MnO_2 TN (456.41 cm^{-1}) might perhaps be attributed to the introduction of Pt into the $[MnO_6]$ unit. This doping of Pt is likely to alter the vibrational frequency of the unit, consequently influencing both the intensity and position of the diffraction peak. The observed displacement of the FTIR spectrum following the introduction of Pt entirely agrees with the findings obtained from XRD analysis. The alignment of the Mn-O network in MnO_2 is notably impacted by the loading of Pt, resulting in deformation of the crystal lattice and a substantial reduction in the crystallinity of the sample. The oxygen exchange capacity of the catalyst is intricately linked to both its crystallinity and the number of defects present. The work conducted by Wang et al.[9] demonstrated that the introduction of Pt loading induces deformation in the Mn-O lattice, resulting in an elevated presence of defects. This phenomenon facilitates the exchange of oxygen and consequently enhances the oxidation process. Therefore, noble metals could infiltrate the crystal lattice of the manganese oxide layer after the reaction, resulting in the creation of lattice imperfections and a decrease in the catalyst's crystallinity.

Meanwhile, The FTIR measurement in Figure 3b findings of Pt/MnO_2 samples with varying Pt loading contents by mass % indicate a steady decrease in the strength of absorption peaks on the spectrum as the Pt loading content increases. The diagram still exhibits the typical absorption band of Mn-O, which is seen at wavelengths of 500 and 700 cm-1. There is a positive correlation between the size of the loading content and the level of noise observed on the baseline. The synthesis of these samples with varying Pt loading amounts was successful, as evidenced by the absence of distinctive peaks corresponding to O-H groups in water and C=O of CO_2.

To examine the morphology of the Pt/MnO_2 material, the synthesized sample was subjected to observation using a scanning electron microscope (SEM). Figure 4 shows that upon Pt loading, the Pt/MnO_2 sample exhibits morphological features that closely resemble those of MnO_2 TN, except for the surface gaps occupied by sheet-shaped particles of varying sizes, ranging from 50 to 100 nm. The nanowire that remains detectable exhibits dimensions ranging from 200 to 600 nm.

The study employed the N_2 isothermal adsorption-release method to examine the impact of Pt loading on the surface of MnO_2, the result is shown in Figure 5 and Figure 6. The findings indicate that the adsorption-desorption pathway of the Pt/MnO_2 sample remains mostly unchanged when MnO_2 is loaded onto the surface of MnO_2. Furthermore, the Pt/MnO_2 sample continues to exhibit the complete features of the MnO_2 TN sample. The N_2 adsorption-release isotherms of both samples may be classified as class IV according to the IUPAC classification, which is particular for mesoporous materials. Additionally, the hysteresis curves are also indicative of this classification—the H_2 form. Capillary condensation occurs when the relative pressure (P/P_o) reaches approximately 0.9. The observed phenomenon can be attributed to the non-baked impregnation procedure, which little alters the material's surface. This outcome aligns entirely with the findings obtained by the scanning electron microscopy (SEM) measurement technique. Nevertheless, the introduction of Pt results in a marginal reduction in the specific surface area of the material. This drop can be attributed to the presence of Pt nanoparticles, which occupy a fraction of the voids on the MnO_2 surface.

The findings in Table 1 indicate that the specific surface areas of three samples, each with varying mass loading levels of Pt (0.5%w, 1%w, and 1.5%w, respectively), exhibit distinct relative surface areas. The specific surface area of the 0.5%Pt sample, as determined by the BET method, is measured to be 93.65 m^2/g. Similarly, the specific surface area of the 1.5%w Pt

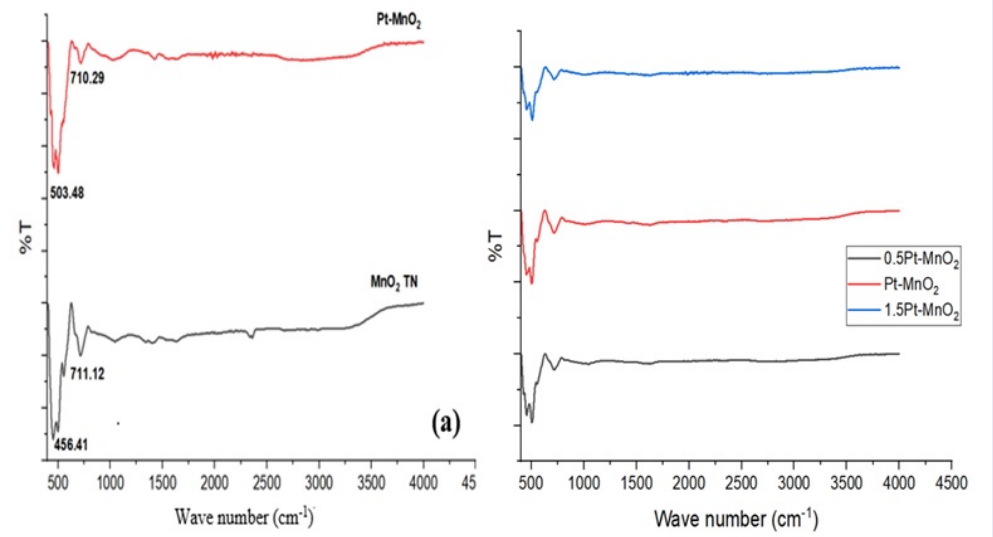

Figure 3: FTIR spectra of (a) Pt/MnO_2 and MnO_2 TN; (b) 0.5Pt/MnO_2, Pt/MnO_2, 1.5Pt/MnO_2

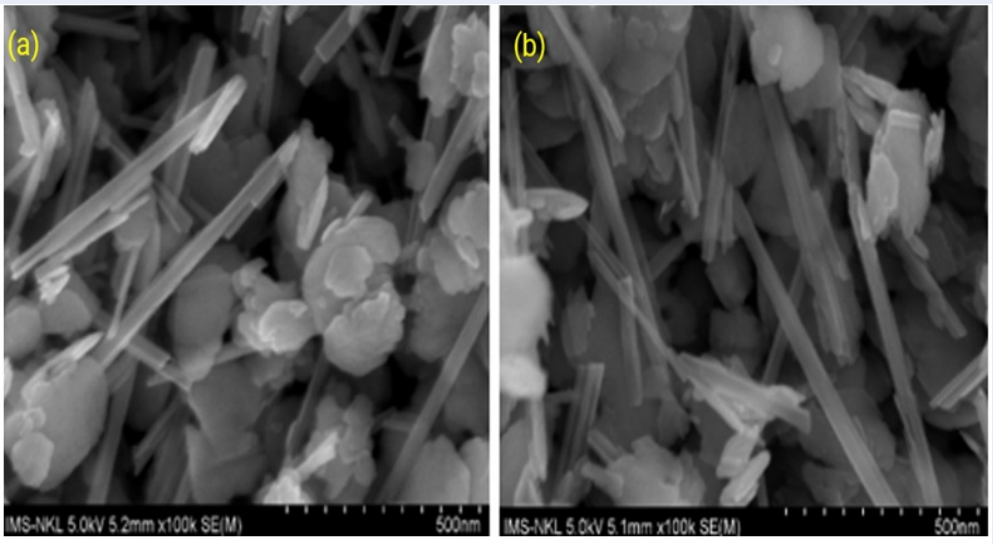

Figure 4: SEM images of (a) MnO_2 TN, (b) Pt/MnO_2

Table 1: Surface porous properties of all samples.

Sample	SBET (m^2/g)	dpore (nm)
MnO_2 TN	113.7	25.76
0.5 Pt/MnO_2	93.65	25.43
Pt/MnO_2	108.74	24.88
1.5 Pt/MnO_2	88.95	27.98

sample is 88.95 m2/g. Notably, the 1%w Pt sample exhibits the highest specific surface area among the three, measuring 108.74 m^2/g.

The pore pattern seen in Figure 6 indicates the presence of medium and large capillaries in all three samples containing Pt. The sample containing 1% platinum exhibited the most significant proportion of pores ranging in diameter from 2 to 10 nanometers. The two remaining samples show comparable pore size distributions.

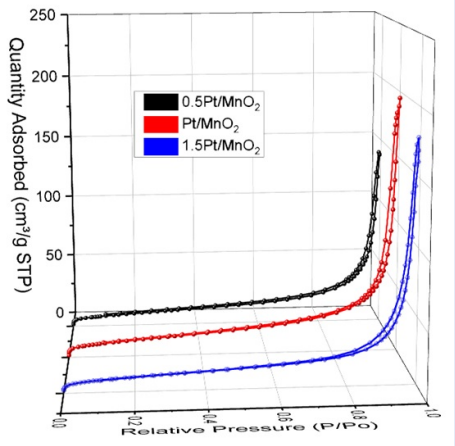

Figure 5: N_2 adsorption-desorption isotherms of all sample MnO_2

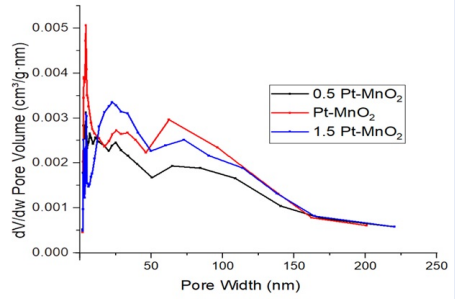

Figure 6: Capillary distribution curves of Pt/MnO_2 samples with different loading Pt contents

Energy Dispersive X-ray Spectroscopy (EDS) analysis on Table 2 reveals that the Pt content deposited on MnO_2 amounts to 1.01%, a value that closely aligns with the theoretical calculation. The platinum (Pt) content was uniformly distributed across the material's surface, maintaining a precise mass fraction of 1%. Regarding the MnO_2 TN sample, the analysis revealed the presence of peaks corresponding to the elements Mn and O. This suggests that the synthesis procedure effectively eliminated additional components, such as potassium (K) from $KMnO_4$ and sulfur (S) from $MnSO_4$, which were likely washed away during the sample preparation. The hydrothermal approach facilitates the synthesis of MnO_2 with a high degree of purity, devoid of any additional contaminants. Based on the observations above, it can be inferred that Pt was effectively transferred onto MnO_2, and the impregnation technique effectively facilitated the deposition of Pt particles onto the material's surface.

Catalytic activity

To examine the catalytic activity of the as-prepared catalysts, the toxic gas toluene was used as a model for catalytic oxidation. The experiments involved the complete oxidation of 6000 ppm of benzene vapor at a GHSV of 11000 h^{-1}. The results are illustrated in Figure 7.

Based on the conversion graph in Figure 7, it is evident that the utilization of Pt as a catalyst, despite its mere 1% mass loading, has led to a substantial enhancement in the conversion of the toluene oxidation reaction, surpassing the conventional transition metal oxide catalyst, such as Manganese oxide. When MnO_2 TN is present, it exhibits the capability to fully toluene convert at a temperature of 300 ^oC. However, by using a catalyst consisting of only 1% Pt by weight, the total conversion of toluene can be achieved at a significantly lower temperature of 190 ^oC. The graphs depicting the behavior of the two catalysts exhibit a high degree of similarity. This can be attributed to the fact that, during the initial stage, both catalysts primarily engage in the adsorption and oxidation of toluene, forming various intermediate molecules. The CO_2 selectivity of the MnO_2 TN catalyst sample showed a complete attainment of 100% at a temperature of 300 degrees Celsius. In contrast, the CO_2 selectivity of Pt/MnO_2 exhibited the ability to achieve a complete 100% selectivity starting from a lower temperature of 170 degrees Celsius. The results indicate that the Pt/MnO_2 catalyst effectively facilitated the extensive oxidation of toluene, resulting in the formation of less harmful byproducts such as CO_2 and H_2O, hence mitigating the occurrence of secondary pollution.

As we can see in Figure 8, the catalytic efficacy of manganese oxide is contingent upon various aspects, including the composition of oxygen within the network, the presence of vacant oxygen sites and adsorbed oxygen species, the surface area, and the oxidation state, among others. These factors exhibit a

Table 2: EDS analysis of MnO_2TN and Pt/MnO_2

MnO_2 TN		
Element	Mass %	Atom %
O	43.36	72.44
Mn	56.64	27.56
Pt	-	-
Total	100.00	100.00
Pt/MnO2		
O	35.73±3.63	49.80±5.05
Mn	24.92±2.45	22.86±2.24
Pt	12.48±1.95	10.31±1.61
Total	100.00	100.00

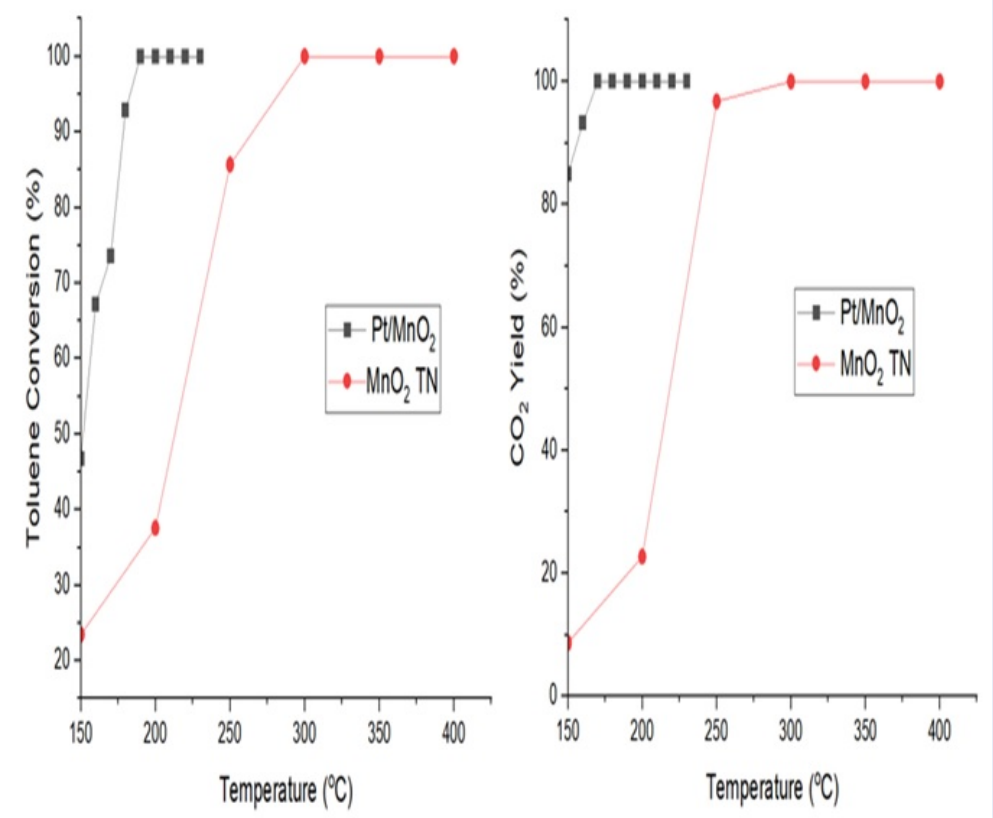

Figure 7: Profile of Toluene conversion over MnO_2TN and Pt/MnO_2 and CO_2 yield over MnO_2TN and Pt/MnO_2

strong correlation. The adsorption density of oxygen is positively correlated with the concentration of manganese in its high oxidation state (Mn^{4+}). Conversely, an increase in the quantity of manganese in its low oxidation state (Mn^{2+}) leads to an increase in the density of oxygen vacancies. The impact of oxidation state distribution on the catalytic activity of manganese oxide has been demonstrated by Tang et al.[36]. Specifically, the ratio of Mn^{2+}/Mn^{4+} has been identified as a crucial factor influencing the material's catalytic activity. The author has demonstrated that manganese oxide displays optimal activity when the ratio of Mn^{2+}/Mn^{4+} approaches unity. The redox mechanism plays a crucial role in the oxidation of BTX on manganese oxide $Mn^{4+} \leftrightarrow Mn^{3+} \leftrightarrow Mn^{2+}$ at this particular ratio, facilitating a smooth reaction. Consequently, introducing Pt onto the catalyst surface induces robust metal support interactions between noble metals and metal oxide support materials, enhancing catalytic performance. Sengpeng et al.[37] made evidence in their study that including Pt on the surface of MnO_2 decreases the links between Mn and O atoms, hence enhancing the mobility of oxygen within the network. The presence of crystals on the catalyst surface can facilitate the efficient oxidation of toluene, even at very moderate temperatures. This phenomenon may explain the substantial disparity observed in the conversion rate.

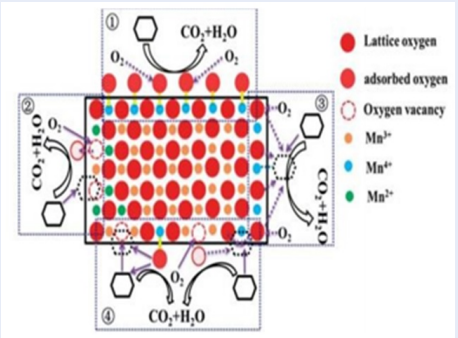

Figure 8: Possible mechanism with oxidation reaction on manganese oxide

A set of experiments was performed on a microflow system to evaluate the efficacy of the catalysts. The system had a total gas flow rate of 60 ml/min and a volume rate of 11000 h^{-1}. The specimens were placed at the midpoint of the reaction tube, each weighing 0.1 gram, and subjected to a toluene treatment with a concentration of 9000 ppm. Figure 9 displays the outcomes of an investigation into the catalytic activity

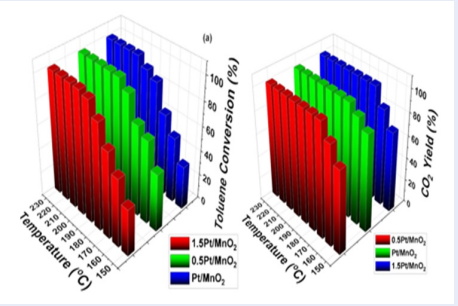

Figure 9: Profile of (a) Toluene conversion over 0.5PT/MnO_2, Pt/MnO_2 and 1.5PT/MnO_2; (b) CO_2 yield over 0.5PT/MnO_2, Pt/MnO_2 and 1.5PT/MnO_2

of Pt/MnO_2 samples with varying Pt concentrations in the process of toluene oxidation.

Based on the findings derived from the analysis of catalytic activity in the microflow system, as depicted in Figure 9, it is evident that the conversion efficiency of the examined samples exhibits a progressive increase in the following sequence: 1.5Pt/MnO_2 < 0.5Pt/MnO_2 < Pt/MnO_2. This outcome can be elucidated in full accordance with the findings of the distinctive measuring experiments done. The Pt/MnO_2 sample possesses a crystalline structure characterized by the presence of rods and particles, which contributes to its substantial specific surface area and notable porosity. Consequently, this structural configuration enhances the catalyst's ability to adsorb oxygen and toluene on its surface, facilitating these substances' absorption. The Pt/MnO_2 catalyst model has enhanced efficacy in facilitating the oxidation process of toluene. It demonstrates the capability to achieve complete conversion of toluene at a temperature of 190 ^oC, while also attaining a CO_2 selectivity of 100% at 170 ^oC.

A series of tests were conducted to investigate the catalytic stability, including a catalytic activity test conducted at a temperature of 190 ^oC. However, it is worth noting that during this test, the catalyst was subjected to continuous testing for a duration of 10 hours.

Based on the findings of the catalytic durability investigation, it is evident from Figure 10 that the Pt/MnO_2 catalyst required an initial stabilization period of 50 minutes. During the initial phase of the reaction, the conversion rate ranges from 88% to 96%. This is mainly attributed to the adsorption of toluene and oxygen from the gas stream onto the surface. However, the quantity of oxygen adsorbed remains insufficient for the complete oxidation of toluene. The CO_2

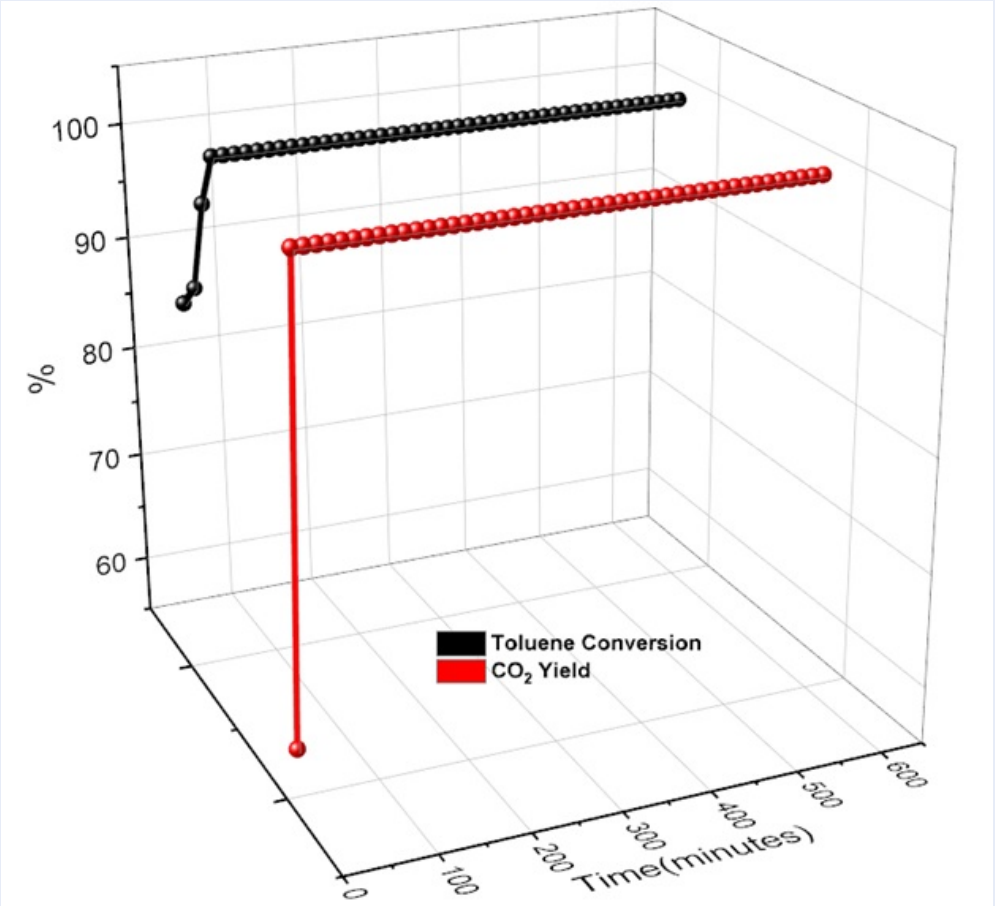

Figure 10: Profile of Toluene conversion over CO_2 yield over Pt/MnO_2 for 600 minutes continuous test.

selectivity graph reveals a notable trend during the initial 12.75-minute interval. Specifically, the CO_2 selectivity is noted to be merely 60%, while the toluene conversion attains a significantly higher value of 88%. This indicates that the majority of the toluene is primarily digested. The primary factor contributing to this phenomenon is the adsorption process occurring on the surface, coupled with oxidation. However, it is essential to note that this process yields intermediate products rather than complete oxidation, producing CO_2 and H_2O. Throughout the duration spanning from 50 minutes to 10 hours, the conversion and selectivity of CO_2 remained consistently high at 100%. Notably, no discernible variations were seen during the activity test. The Pt/MnO_2 catalyst has commendable characteristics and demonstrates notable temperature stability. Due to the relatively mild reaction conditions maintained at a temperature of 190 ^oC, there remains a lack of observable indications pertaining to the sintering or clustering of Pt particles. Consequently, the catalytic activity of the catalyst is minimally impacted.

CONCLUSION

To assess the catalytic efficacy of platinum in conjunction with manganese oxide, a range of Pt/MnO_2 samples with varying mass fractions of platinum were synthesized, described, and subjected to testing for the complete oxidation of toluene. The Pt/MnO_2 catalyst containing one wt% of platinum exhibited superior catalytic performance compared to the toluene oxidation activity in the other samples. Additionally, it shows the most significant surface area. The active phase for toluene oxidation in Pt/MnO_2 was determined to be Pt. The robust interaction between the noble metal platinum (Pt) and manganese oxide (MnO_2) contributes to the enhanced stability of the Pt/MnO_2 oxide catalyst during oxidation processes.

ACKNOWLEDGMENT

This work was financially supported by the Ministry of Natural Resources and Environment. The project No TNMT.2022.05.04.

LIST OF ABBREVIATIONS

Ppm: point per million
GHSV: Gas hourly space velocity
VOCs: volatile organic compounds

CONFLICT OF INTERESTS STATEMENT

The authors want to make sure that there is no conflict of interest in the article's publication.

CREDIT AUTHORSHIP CONTRIBUTION STATEMENT

Tran Van Hien: Conceptualization, Validation, Supervision, Project administration, Funding acquisition.

Ha Quoc Bang: Conceptualization, Methodology, Validation, Supervision, Writing – review & editing

Khong Manh Hung: Methodology, Data curation, Formal analysis, Resources, Investigation, Writing – review & editing.

REFERENCES

1. Yang C, Miao G, Pi Y, Xia Q, Wu J, Li Z, Xiao J. Abatement of various types of VOCs by adsorption/catalytic oxidation: A review. Chem Eng J. 2019;370:1128-1153;Available from: https://doi.org/10.1016/j.cej.2019.03.232.
2. Kamal MS, Razzak SA, Hossain MM. Catalytic oxidation of volatile organic compounds (VOCs)-A review. Atmos Environ. 2016;140:117-134;Available from: https://doi.org/10.1016/j.atmosenv.2016.05.031.
3. Wu P, Jin X, Qiu Y, Ye D. Recent progress of thermocatalytic and photo/thermocatalytic oxidation for VOCs purification over manganese-based oxide catalysts. Environ Sci Technol. 2021;55(8):4268-4286;PMID: 33720707. Available from: https://doi.org/10.1021/acs.est.0c08179.
4. Gu W, Li C, Qiu J, Yao J. Facile fabrication of flower-like MnO2 hollow microspheres as high-performance catalysts for toluene oxidation. J Hazard Mater. 2021;408:124458;PMID: 33168316. Available from: https://doi.org/10.1016/j.jhazmat.2020.124458.
5. Zhang X, Gao B, Creamer AE, Cao C, Li Y. Adsorption of VOCs onto engineered carbon materials: A review. J Hazard Mater. 2017;338:102-123;PMID: 28535479. Available from: https://doi.org/10.1016/j.jhazmat.2017.05.013.
6. Zhang C, Gao X, Qin J, Guo Q, Zhou H, Jin W. Microporous polyimide VOC-rejective membrane for separating nitrogen/VOC mixture. J Hazard Mater. 2021;402:123817;PMID: 33254806. Available from: https://doi.org/10.1016/j.jhazmat.2020.123817.
7. Zhang S, You J, Kennes C, Cheng Z, Ye J, Chen D, Chen J, Wang L. Current advances of VOCs degradation by bioelectrochemical systems: a review. Chem Eng J. 2018;334:2625-2637;Available from: https://doi.org/10.1016/j.cej.2017.11.014.
8. Guo Y, Wen M, Li G, An T. Recent advances in VOC elimination by catalytic oxidation technology onto various nanoparticles catalysts: a critical review. Appl Catal B. 2021;281:119447;Available from: https://doi.org/10.1016/j.apcatb.2020.119447.
9. Qin Y, Wang Y, Li J, Qu Z. Effect of Ag on toluene oxidation over Ag supported wire-like MnO2 catalysts. Surf Interfaces. 2020;21:100657;Available from: https://doi.org/10.1016/j.surfin.2020.100657.
10. Xiong S, Huang N, Peng Y, Chen J, Li J. Balance of activation and ring-breaking for toluene oxidation over CuO-MnOx bimetallic oxides. J Hazard Mater. 2021;415:125637;PMID: 33740717. Available from: https://doi.org/10.1016/j.jhazmat.2021.125637.
11. Ma M, Zhu Q, Jiang Z, Jian Y, Chen C, Liu Q, He C. Achieving toluene efficient mineralization over K/α-MnO2 via oxygen vacancy modulation. J Colloid Interface Sci. 2021;598:238-249;PMID: 33901849. Available from: https://doi.org/10.1016/j.jcis.2021.04.043.
12. Guo N, Zhang J, Jiang L, Wang D, Wang Z. Highly efficient and selective Ru and Ce modified ZSM-5 catalysts for catalytic oxidation of toluene. Colloids Surf A. 2022;651:129709;Available from: https://doi.org/10.1016/j.colsurfa.2022.129709.
13. Shi Z, Yang P, Tao F, Zhou R. New insight into the structure of CeO2-TiO2 mixed oxides and their excellent catalytic performances for 1, 2-dichloroethane oxidation. Chem Eng J. 2016;295:99-108;Available from: https://doi.org/10.1016/j.cej.2016.03.032.
14. Hu F, Chen J, Peng Y, Song H, Li K, Li J. Novel nanowire self-assembled hierarchical CeO2 microspheres for low-temperature toluene catalytic combustion. Chem Eng J. 2018;331:425-434;Available from: https://doi.org/10.1016/j.cej.2017.08.110.
15. Zhang J, Li Y, Wang L, Zhang C, He H. Catalytic oxidation of formaldehyde over manganese oxides with different crystal structures. Catal Sci Technol. 2015;5(4):2305-2313;Available from: https://doi.org/10.1039/C4CY01461H.
16. Wen M, Mori K, Kuwahara Y, An T, Yamashita H. Design and architecture of metal-organic frameworks for visible light-enhanced hydrogen production. Appl Catal B. 2017;218:555-569;Available from: https://doi.org/10.1016/j.apcatb.2017.06.082.
17. Ye Z, Giraudon J-M, De Geyter N, Morent R, Lamonier J-F. The design of MnOx based catalyst in post-plasma catalysis configuration for toluene abatement. Catalysts. 2018;8(2):91;Available from: https://doi.org/10.3390/catal8020091.
18. Bo Z, Yang S, Kong J, Zhu J, Wang Y, Yang H, Li X, Yan J, Cen K, Tu X. Solar-enhanced plasma-catalytic oxidation of toluene over a bifunctional graphene fin foam decorated with nanofin-like MnO2. ACS Catal. 2020;10(7):4420-4432;PMID: 32296596. Available from: https://doi.org/10.1021/acscatal.9b04844.
19. Dinh MT, Giraudon J-M, Vandenbroucke AM, Morent R, De Geyter N, Lamonier J-F. Manganese oxide octahedral molecular sieve K-OMS-2 as catalyst in post-plasma-catalysis for trichloroethylene degradation in humid air. J Hazard Mater. 2016;314:88-94;PMID: 27107238. Available from: https://doi.org/10.1016/j.jhazmat.2016.04.027.
20. Subrahmanyam Ch, Renken A, Kiwi-Minsker L. Catalytic nonthermal plasma reactor for abatement of toluene. Chem Eng J. 2010;160(2):677-682;Available from: https://doi.org/10.1016/j.cej.2010.04.011.
21. Sultana S, Vandenbroucke AM, Mora M, Jiménez-Sanchidrián C, Romero-Salguero FJ, Leys C, De Geyter N, Morent R. Post-plasma-catalysis for trichloroethylene decomposition over CeO2 catalyst: Synergistic effect and stability test. Appl Catal B. 2019;253:49-59;Available from: https://doi.org/10.1016/j.apcatb.2019.03.077.
22. Dhandapani B, Oyama ST. Gas phase ozone decomposition catalysts. Appl Catal B. 1997;11(2):129-166;Available from: https://doi.org/10.1016/S0926-3373(96)00044-6.
23. Li Y, Fan Z, Shi J, Liu Z, Shangguan W. Post plasma-catalysis for VOCs degradation over different phase structure MnO2 catalysts. Chem Eng J. 2014;241:251-258;Available from: https://doi.org/10.1016/j.cej.2013.12.036.

24. Liang S, Teng F, Bulgan G, Zong R, Zhu Y. Effect of phase structure of MnO2 nanorod catalyst on the activity for CO oxidation. J Phys Chem C. 2008;112(14):5307-5315;Available from: https://doi.org/10.1021/jp0774995.
25. Yusuf S, Neal LM, Li F. Effect of promoters on manganese-containing mixed metal oxides for oxidative dehydrogenation of ethane via a cyclic redox scheme. ACS Catal. 2017;7(8):5163-5173;Available from: https://doi.org/10.1021/acscatal.7b02004.
26. Dinh MT, Giraudon J-M, Vandenbroucke AM, Morent R, De Geyter N, Lamonier J-F. Post plasma-catalysis for total oxidation of trichloroethylene over Ce-Mn based oxides synthesized by a modified "redox-precipitation route". Appl Catal B. 2015;172:65-72;Available from: https://doi.org/10.1016/j.apcatb.2015.02.013.
27. Jiang N, Qiu C, Guo L, Shang K, Lu N, Li J, Zhang Y, Wu Y. Plasma-catalytic destruction of xylene over Ag-Mn mixed oxides in a pulsed sliding discharge reactor. J Hazard Mater. 2019;369:611-620;PMID: 30825807. Available from: https://doi.org/10.1016/j.jhazmat.2019.02.087.
28. Yi H, Miao L, Xu J, Zhao S, Xie X, Du C, Tang T, Tang X. Palladium particles supported on porous CeMnO3 perovskite for catalytic oxidation of benzene. Colloids Surf A. 2021;623:126687;Available from: https://doi.org/10.1016/j.colsurfa.2021.126687.
29. Chen L, Jia J, Ran R, Song X. Nickel doping MnO2 with abundant surface pits as highly efficient catalysts for propane deep oxidation. Chem Eng J. 2019;369:1129-1137;Available from: https://doi.org/10.1016/j.cej.2019.03.142.
30. Kim J, Kwon EE, Lee JE, Jang S-H, Jeon J-K, Song J, Park Y-K. Effect of zeolite acidity and structure on ozone oxidation of toluene using Ru-Mn loaded zeolites at ambient temperature. J Hazard Mater. 2021;403:123934;PMID: 33264983. Available from: https://doi.org/10.1016/j.jhazmat.2020.123934.
31. Lin T, Yu L, Sun M, Cheng G, Lan B, Fu Z. Mesoporous α-MnO2 microspheres with high specific surface area: Controlled synthesis and catalytic activities. Chem Eng J. 2016;286:114-121;Available from: https://doi.org/10.1016/j.cej.2015.09.024.
32. He C, Cheng J, Zhang X, Douthwaite M, Pattisson S, Hao Z. Recent advances in the catalytic oxidation of volatile organic compounds: a review based on pollutant sorts and sources. Chem Rev. 2019;119(7):4471-4568;PMID: 30811934. Available from: https://doi.org/10.1021/acs.chemrev.8b00408.
33. Chen C, Zhu J, Chen F, Meng X, Zheng X, Gao X, Xiao F-S. Enhanced performance in catalytic combustion of toluene over mesoporous Beta zeolite-supported platinum catalyst. Appl Catal B. 2013;140:199-205;Available from: https://doi.org/10.1016/j.apcatb.2013.03.050.
34. Peng R, Li S, Sun X, Ren Q, Chen L, Fu M, Wu J, Ye D. Size effect of Pt nanoparticles on the catalytic oxidation of toluene over Pt/CeO2 catalysts. Appl Catal B. 2018;220:462-470;Available from: https://doi.org/10.1016/j.apcatb.2017.07.048.
35. Zhang H, Sui S, Zheng X, Cao R, Zhang P. One-pot synthesis of atomically dispersed Pt on MnO2 for efficient catalytic decomposition of toluene at low temperatures. Appl Catal B. 2019;257:117878;Available from: https://doi.org/10.1016/j.apcatb.2019.117878.
36. Tang W, et al. Oxalate route for promoting activity of manganese oxide catalysts in total VOCs' oxidation: effect of calcination temperature and preparation method. J Mater Chem A. 2014;2(8):2544-2554;Available from: https://doi.org/10.1039/C3TA13847J.
37. Wu Y, et al. A novel redox-precipitation method for the preparation of α-MnO2 with a high surface Mn4+ concentration and its activity toward complete catalytic oxidation of o-xylene. Catal Today. 2013;201:32-39;Available from: https://doi.org/10.1016/j.cattod.2012.04.032.

Tạp chí Phát triển Khoa học và Công nghệ – Engineering and Technology 2024, 6(SI3):34-45

Open Access Full Text Article

Bài nghiên cứu

Xúc tác trên MnO_2 được kết hợp Pt để cải thiện quá trình oxi hóa VOCs

Khổng Mạnh Hùng*, Trần Văn Hiền, Hà Quốc Bảng

TÓM TẮT

Một trong những nguyên nhân hàng đầu gây ô nhiễm không khí đó chính là các hợp chất hữu cơ dễ bay hơi (VOCs), các hợp chất này không những gây nguy hiểm nghiêm trọng cho môi trường mà còn ảnh hưởng sức khỏe con người. Quá trình oxy hóa xúc tác đã được công nhận là một phương pháp đầy hứa hẹn và thành công để xử lý VOC. Do giá cả phải chăng và tính thân thiện với môi trường, oxit gốc mangan là một trong những lựa chọn không thể bỏ qua để phân hủy VOCs bằng xúc tác. Trong nghiên cứu này, chúng tôi phân tán Pt trên MnO_2 với hàm lượng về khối lượng của Pt lần lượt là 0,5, 1 và 1,5% để kiểm soát sự tương tác của Pt-MnO_2. So với MnO_2, chất xúc tác Pt-MnO_2 thể hiện hiệu suất oxy hóa VOC cao hơn do diện tích bề mặt Brunauer-Emmett-Teller cao, oxy mạng hoạt động mạnh hơn, các nguyên tử Pt tiếp xúc nhiều hơn. Trong số tất cả các mẫu thực vật được tạo ra với tỷ lệ khối lượng khác nhau, mẫu Pt-MnO2 thể hiện các đặc tính cũng như hoạt tính xúc tác tốt nhất. Diện tích bề mặt riêng của Pt-MnO2 là 108,74 m2/g. Chất xúc tác Pt-MnO2 có thể chuyển đổi hoàn toàn Toluene thành CO2 và H2O ở nhiệt độ thấp hơn chỉ 190 C mà vẫn duy trì độ ổn định cao trong 600 phút. Trong điều kiện tốc độ không gian cao, hiệu suất của chất xúc tác Pt-MnO_2 trong quá trình oxy hóa VOC tương đối ổn định, cho thấy triển vọng to lớn khi sử dụng trong thực tiễn. Nghiên cứu này cho thấy chất xúc tác MnO_2 phân tán Pt vượt trội hơn chất xúc tác MnO_2 thông thường trong quá trình oxy hóa VOCs.

Từ khoá: Mangan oxit, Bạch kim, Toluen, Oxi hóa xúc tác, VOCs

Viện Hóa học-Vật liệu /Viện Khoa học và Công nghệ quân sự, 17 Hoàng Sâm, Phường Nghĩa Đô, Quận Cầu Giấy, Hà Nội

Liên hệ

Khổng Mạnh Hùng, Viện Hóa học-Vật liệu /Viện Khoa học và Công nghệ quân sự, 17 Hoàng Sâm, Phường Nghĩa Đô, Quận Cầu Giấy, Hà Nội

Email: Hungkhong123123@gmail.com

Lịch sử

- Ngày nhận: 31-8-2023
- Ngày chấp nhận: 03-1-2024
- Ngày đăng: 31-3-2024

DOI : https://doi.org/10.32508/stdjet.v6iSI3.1189

Trích dẫn bài báo này: Hùng K M, Hiền T V, Bảng H Q. **Xúc tác trên MnO_2 được kết hợp Pt để cải thiện quá trình oxi hóa VOCs**. *Sci. Tech. Dev. J. - Eng. Tech.* 2024, 6(SI3):34-45.